First-Principle Calculations on the Microscopic Fe-57 Electric-Field-Gradient Tensor of Ferrous Chloride Tetrahydrate: A Prototypical Mossbauer Species

ARTICLE *in* THE JOURNAL OF PHYSICAL CHEMISTRY A · AUGUST 2011

Impact Factor: 2.69 · DOI: 10.1021/jp206218g · Source: PubMed

3 AUTHORS, INCLUDING:

James N. Bull
University of Melbourne
23 PUBLICATIONS **76** CITATIONS
SEE PROFILE

William Tennant
University of Canterbury
58 PUBLICATIONS **625** CITATIONS
SEE PROFILE

THE JOURNAL OF PHYSICAL CHEMISTRY A

ARTICLE

pubs.acs.org/JPCA

First-Principle Calculations on the Microscopic ^{57}Fe Electric-Field-Gradient Tensor of Ferrous Chloride Tetrahydrate: A Prototypical Mössbauer Species

James N. Bull,*,† Robert G. A. R. Maclagan,‡ and W. Craighead Tennant‡

†Chemistry Research Laboratory, Department of Chemistry, University of Oxford, 12 Mansfield Road, Oxford OX1 3TA, United Kingdom

‡Department of Chemistry, University of Canterbury, Christchurch 8140, New Zealand

ABSTRACT: Since the pioneering work on the theoretical description of Mössbauer quadrupole line intensities for a single-crystal to elucidate information on the electric-field-gradient (EFG) tensor, ferrous chloride tetrahydrate, $FeCl_2 \cdot 4H_2O$, has represented a prototypical Mössbauer species. In addition, this species also typifies a so-called ambiguous, low symmetry, iron center where traditionally only macroscopic tensors have been assumed available for determination. Recent experiments on $FeCl_2 \cdot 4H_2O$ have successfully determined physically meaningful spin-Hamiltonian parameters for the ^{57}Fe microscopic (local) EFG and mean-squared displacement tensors. This paper reports a density functional theory investigation that finds good agreement with experiment. Assuming a gas-phase scaffold cluster approach to describe the crystalline geometry, the sign of the EFG was determined to be positive, in agreement with earlier magnetically perturbed experiments, and the EFG asymmetry parameter η was calculated to be 0.21−0.23 depending on the density functional used, which is in excellent accord with experiment at 0.25(2). By virtue of theoretical and experimental agreement, this work indicates that simultaneous electric-field-gradient-mean-square-displacement Mössbauer determinations can resolve the apparent ambiguity associated with monoclinic, $2/m$ or $\bar{1}$ Laue class, sites provided there is sufficient anisotropy in the Lamb−Mössbauer recoilless fraction.

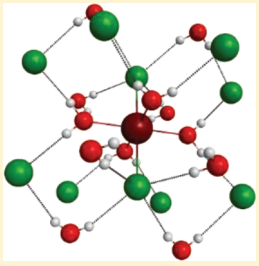

1. INTRODUCTION

A point charge q at distance $r = (x^2 + y^2 + z^2)^{1/2}$ from a nucleus may cause a potential $V(r) = q/r$ at the nucleus. The associated electric field $\mathbf{E}$ at the nucleus is the negative gradient of the potential, $-\nabla\mathbf{V}$, and the electric-field-gradient (EFG) is given by

$$\mathrm{EFG} = \nabla\mathbf{E} = -\nabla\nabla\mathbf{V} = \begin{pmatrix} V_{xx} & V_{xy} & V_{xz} \\ V_{yx} & V_{yy} & V_{yz} \\ V_{zx} & V_{zy} & V_{zz} \end{pmatrix} \quad (1)$$

where

$$V_{ij} = \frac{\partial^2 \mathbf{V}}{\partial r_i \partial r_j} \qquad (i, j = x, y, z) \quad (2)$$

and 1 au = 9.717365 × 10^{21} V m^{-2}. Because the EFG is symmetric and traceless (cf. Laplace equation), there are only five independent V_{ij} components. In a crystalline solid, the EFG at the point of a nucleus can be considered to arise from two sources: valence bonding electrons and their spatial symmetry charge anisotropy (the major source) and second-coordination shell or lattice charges (the minor source). When a Mössbauer nucleus possesses nuclear spin $I > 1/2$, the resulting nuclear electric quadrupole moment, Q, can couple with a nonzero EFG at the nucleus to yield a hyperfine quadrupole splitting. For ^{57}Fe this interaction is measurable by Mössbauer spectroscopy through the 14.41 keV ($I = 1/2 \leftrightarrow I = 3/2$) nuclear transition. Convention expresses the EFG in terms of the largest eigenvalue, $V_{\hat{z}\hat{z}}$ (=$eq_{\hat{z}\hat{z}}$ where e is the elementary charge, $e = 1$ in au), and the asymmetry parameter, η, defined as

$$\eta = \frac{V_{\hat{x}\hat{x}} - V_{\hat{y}\hat{y}}}{V_{\hat{z}\hat{z}}} \quad (3)$$

where $|V_{\hat{z}\hat{z}}| > |V_{\hat{y}\hat{y}}| \geq |V_{\hat{x}\hat{x}}|$, so that $0 \leq \eta \leq 1$ (i.e., $\eta = 0$ defines the parameter as uniaxial). In 14.41 keV ^{57}Fe Mössbauer, the quadrupole splitting interaction, which is the spectral difference between the $I = 3/2$ Kramers doublet $M_I = \pm 3/2$ and $\pm 1/2$ states and denoted here as ΔE_Q, in conventional spectrum units of mm s^{-1} (a 14.41 keV transition Doppler shift of 1 mm s^{-1} = 4.805 × 10^{-8} eV; 27.2107 eV = 1 au), is given by

$$\Delta E_Q = \frac{eQ}{2} V_{\hat{z}\hat{z}} \left(1 + \frac{\eta^2}{3}\right)^{1/2} \quad (4)$$

where Q is the ^{57m}Fe($I = 3/2$) nuclear electric quadrupole moment with value 150−160 mb (1 mb = 10^{-31} m^2).[1−3]

Recently, Bull et al.[4,5] have reported experiments on the determination of symmetry-related microscopic (individual site or "local") EFGs, for single crystals of the prototypical ferrous chloride tetrahydrate (FCL), $FeCl_2 \cdot 4H_2O$, and ferrous ammonium

Received: July 1, 2011
Revised: August 12, 2011
Published: August 12, 2011

sulfate hexahydrate, $Fe(NH_4)_2(SO_4)_2 \cdot 6H_2O$, species, where for each, the two symmetry-related sites in the $P2_1/c$ unit cell contribute to the same Mössbauer quadrupole doublet. Traditionally, it was thought that, at best, only a manifold of possible microscopic solutions was obtainable, where each set in the manifold averages to the same experimentally measurable macroscopic EFG.[6−8] The microscopic resolution method relied on addition of the next-largest, anisotropic, interaction to the spin-Hamiltonian, that is, the mean-squared-displacement (MSD).[9] Application involved simultaneously refining a Mössbauer radiation-intensity quantum vector coupling model to a series of single-crystal measurements. The final refinements gave excellent accord between calculated model and thin-crystal-limit corrected experimental data, and it was shown that systematic variation of initial trial parameters always gave convergence to the same solution indicating a single global fit. It would, however, be highly desirable to have first principle quantum chemical (density functional theory) calculations in support of these determinations.

Wave function ab initio calculation of ^{57}Fe, or generally d-block EFGs, is difficult due to degeneracies and the need for a multiconfigurational description. Alternatively, due to the rapid development of efficient density functional methods coupled with ever-increasing computational power, the past few years has seen considerable interest in the ability of DFT to theoretically calculate EFG tensors.[10,11] These studies can be divided into two categories. The first category encompasses studies that have attempted to calculate EFGs for a few similar species and were correlated with experimental ΔE_Q (or nuclear quadrupole coupling constants) to extrapolate for nuclear quadrupole moments and have provided what has been accepted as the most accurate values of $Q(^{57m}Fe)$ = 150−160 mb using either relativistic or nonrelativistic theories.[1−3,12,13] Extrapolation specifically considering the influence of scalar and spin−orbit relativistic corrections to calculated EFGs indicate Q is essentially invariant at Q(nonrelativistic) = 158(14) mb and Q(relativistic) = 156(13) mb.[12,13] It appears that, unlike for Cu or heavier halides,[14−18] the ∼6−10% error in $Q(^{57m}Fe)$ is substantially larger than the average relativistic EFG correction. The second category incorporates studies that provide systematic high-level calculations to determine EFG and then ΔE_Q with an assumed Q as to investigate the various levels of theory and their contributions, which have, unsurprisingly, identified the raft of different theoretical parameters requiring careful consideration for a given system. These parameters include a sufficiently large and polarized all-electron basis that considers the nuclear cusp condition,[19−25] sufficient electron correlation,[12,20,21] the ratio of Hartree−Fock to function exchange and associated description of the d−d and HOMO−LUMO energy splitting,[14,16,21−24,26] the use of gas-phase optimized vs X-ray geometries,[12,22,23] and the extent of the coordination shell or scaffold to incorporate.[12,16,27] Gas-phase calculations are only applicable when solid-state complexes have discrete octahedra and little inter-octahedron interactions. When the foregoing is not the case, the use of either scaffold approaches or solid-state periodic type calculations is required.[1,27−32] The scaffold, otherwise known as the cluster/supramolecular approach, approximates the periodic structure of a compound as a cluster molecule. The conclusions on the incorporation of relativistic corrections for ^{57}Fe EFG (or even the use of DFT) calculations change if one wishes to consider an accurate description of shorter-ranged Fermi-contact related properties, arising from the isotropic contribution to hyperfine coupling constants rather than quadrupolar, such as the Mössbauer isomer shift.[25,33] Also outlined in recent studies is the importance of an accurate core tight s-orbital description and numerical radial integration grid coarseness for the isotropic component.[25,33] Symmetry of a quadrupolar interaction requires a sufficiently fine angular description of the DFT numerical integration grid.

In general, both experimental and calculated EFGs are sensitive to subtle geometrical changes and ferrous ΔE_Q's usually exhibit strong temperature dependence.[34,35] The previous EFG experiments of Bull et al.[4,5] were performed at 295(2) K, whereas calculations model 0 K conditions and assume thermal vibrational and librational smearing is small. Fortunately, for FCL, the experimental ΔE_Q change over the 0−300 K range is negligibly small indicating no substantial change in the EFG.

This article endeavors to perform first-principle Gaussian basis set DFT calculations in support of the above-mentioned single-crystal ^{57}Fe Mössbauer EFG determinations for three reasons: (i) to confirm the sign of the EFG as positive for FCL; (ii) to find support for a value of microscopic η for FCL; (iii) to assess the simultaneous EFG-MSD experimental determination method through comparisons with calculated EFG. This paper is ordered as follows. First, appropriate bases used on each atom and DFT functionals are outlined. Performance was characterized on the basis of calculations with the CuCl and $FeCl_2$ species. Following, FCL calculations assuming one octahedron and the scaffold approach are presented and results are discussed in comparison with experiments. Finally, it is shown that the assumed X-ray octahedron geometry in the scaffold is very close to the energy minimum, and both ΔE_Q and η are in excellent accord with experiment only near this geometry.

2. METHODS

All gas-phase and scaffold calculations were performed using the GAMESS-US[36] and CFOUR[37] computational packages. The FCL crystallographic geometry was assumed from a recent X-ray redetermination.[38]

Following guidance from the literature studies outlined in the Introduction, these Gaussian basis calculations were approached by systematically varying three variables: basis set, electron correlation/exchange−correlation functional, and unit cell contents. All bases were mainly of the Dunning's type[39−42] and are systematically outlined for Cu or Fe and coordinated Cl atoms in section 3.1 below. Otherwise, O atoms coordinated to the central Fe were treated with the cc-pVTZ basis, and H atoms on coordinated H_2O with the cc-pVDZ basis. Scaffold H, S, N, and O atoms were treated with the cc-pVDZ basis, and scaffold frame Fe and Cl atoms with the smaller TZV basis set.[43] Additional d polarization functions were not important for scaffold frame Cl atoms. For Cu and Fe atoms, additional uncontracted large orbital exponent (i.e., tight) core p and d functions were systematically added in an even-tempered geometric progression series to achieve EFG basis set convergence for gas-phase CuCl and $FeCl_2$. An accurate core description is important as charge contributions to the EFG scale radially as $\langle r^{-3} \rangle$. Although studies have indicated relativistic corrections to not be important for ^{57}Fe EFGs,[12,13] several relativistic integral correction calculations were affected using the Gaussian 09[44] implementation of the second-order (DKH2) and fourth-order (DKH4) Douglas−Kroll−Hess transformation.[45−48] The use of approximate one- or two-component relativistic theories with one-electron expectation

property operators suffers from a so-called picture change error,[18,49] although on the basis of the above studies including one considering a full four-component Dirac Hamiltonian, the ^{57}Fe EFG spin−orbit term, which is proportional to the picture change error, is expected to be small and therefore neglected.

The different density functionals tested, with the fraction of exact Hartree−Fock exchange in parentheses when appropriate, were BHandHLYP (50%) (denoted as BHHLYP herein),[50] B3LYP (20%),[51] CAM-B3LYP,[52] CAM-B3LYP*,[16] PBE0 (25%),[53] ωB97XD,[54] TPSSh (10%),[55] and the recent double-hybrid B2-PLYP (∼50% HF exchange, ∼25% MBPT correlation).[56] The first of these functionals performed, fortuitously, reasonably for CuCl benchmarks and has been shown to give a reasonable description of hydrogen-bonding and charge-transfer nonbonded interactions.[14,21,57] CAM-B3LYP is a long-range corrected variant of B3LYP, and reparameterization of the long-range Coulomb-attenuated component, denoted CAM-B3LYP* (with CAM parameters: $\alpha = 0.4$; $\beta = 0.179$; $\mu = 0.99$), has performed very well for a series of relativistic diatomic EFGs and other gas-phase transition metal nuclear quadrupole coupling measurements.[15,23] The PBE0 functional was originally designed specifically for electric response calculations and has shown good performance for the related main group and, potentially, iron-containing molecular polarizabilities.[58] ωB97XD is a long-range corrected functional that was designed to perform well for nonbonding interactions. TPSSh is generally a favored functional when transition metal systems are treated and has been stated to be at least as accurate as or better than B3LYP for hyperfine parameters.[59] B2PLYP has shown good performance for other Cu and transition metal hyperfine parameters.[33,59,60] DFT calculations performed with GAMESS-US utilized a Lebedev integration grid with 128 radial and 590 angular points. In practice, the smaller and default 96 × 302 grid gave only ∼0.5% differences in computed EFG with the current bases. To ensure the 128 × 590 grid was sufficient for EFGs, several 800 × 1202 ultrafine grid calculations were performed and gave less than 0.1% difference. Calculations using both unrestricted open-shell Kohn−Sham (UKS) and restricted open-shell Kohn−Sham (ROKS) references were performed. UKS methods can suffer from spin contamination, as assessed from consideration of $\langle S^2 \rangle$, and erratic convergence behavior.[25] Though these shortfalls are overcome in ROKS; the latter does not allow for spin polarization effects.

3. RESULTS AND DISCUSSION

3.1. Preliminary Level of Theory: CuCl and $FeCl_2$. As a starting point to establish suitable all-electron bases for metal and Cl atoms, gas-phase optimizations were performed on the CuCl species using the BHHLYP functional.[14,21] Preliminary basis-set testing combined with evaluation of similar work performed on Cd complexes,[19] led to adoption of the all-electron nonrelativistic cc-pwCVTZ Dunnings-type bases,[42] with three additional uncontratcted orbitals (one core p and two core d), with orbital exponents of 2008.7, 512.7, and 1538.1, respectively. These additional core functions gave a ∼14% improvement of the computed CuCl EFG, with further core augmentation showing negligible (<1%) change, indicating near basis set convergence. The additional d orbitals were the most important contributing ∼88% of this improvement and gave EFG convergence to the same value obtained with the unmodified cc-pwCVQZ basis, but at significantly lower computational cost. Similar calculations considering the Cl ligand indicated the calculated EFG difference between treatment with cc-pVTZ and aug-cc-pVTZ bases was small at ∼3%, which is not too surprising considering these functions describe electron density far from the metal nucleus. It needs be noted that the GAMESS-US implementation of the cc-pVTZ basis set for Cl includes an additional set of diffuse uncontracted d functions, which, when removed, made little difference to the EFG. Increasing the Cl basis to cc-pVQZ again gave negligible changes to the computed EFG. The final cc-pwCVTZ-(+p2d)/cc-pVTZ for Cu/Cl basis treatment gave the EFG at −0.331 au, agreeing well with experiment at −0.31(2) au.[61] Basis set superposition errors to the EFG were approximated at ∼0.007 au. In accord with previous studies, geometrically optimized EFG calculations gave wildly ranging values for different functionals, with the numerically next-closest being B2PLYP at −0.355 and −0.352 au with the cc-pwCVTZ-(+p2d)/cc-pVTZ and cc-pwCVQZ/cc-pVTZ bases, respectively. Of interest, CCSD and CCSD(T) cc-pwCVTZ(+p2d)/cc-pVTZ all-electron optimization calculations using package CFOUR gave values of −0.484 and −0.390 au (CCSD(T) dipole moment of 5.495 D in comparison to 5.319 D from relativistic CCSD(T)).[21] These data would indicate perturbative triplets to contribute a significant portion; therefore, a precise benchmark ideally requires CCSDT or better correlation in addition to relativistic and spin−orbit corrections, which are known to be important for Cu.[14,15]

Following from the above calculations, analogous calculations were performed for $FeCl_2$. The central Fe atom used the same additional uncontracted basis augmentation as above, and BHHLYP EFG convergence was similarly found with the cc-pwCVTZ(+p2d)/cc-pVTZ bases for Fe/Cl. Crystalline anhydrous $FeCl_2$ has a sheet-like crystal structure consisting of hexagonal face-centered-cubic layers of chloride ions with interstitial hexagonal layers of ferrous ions between every two layers of chlorides.[62] The coordination of each ferrous ion has 6-fold symmetry and experiences a crystalline field of trigonal symmetry parallel to the crystallographic *c*-axis due to the noncubic lattice arrangement of ferrous ions. This results in the T_{2g} level being split into lower doublet orbitals and a singlet separated by ∼120−150 cm^{-1}, which is close to the small spin−orbit splitting interaction at ∼95 cm^{-1}.[63,64] In accord, the Mössbauer spectrum shows a temperature-dependent ΔE_Q with a magnetic Néel transition at 24 K, and literature ΔE_Q values at 0.80(2) mm s^{-1} at 290 K and 1.30(3) mm s^{-1} at 5 K.[63−66] Measurements below the Néel temperature determined a positive EFG.[63] ^{57}Fe enriched matrix isolation experiments have obtained ΔE_Q at 0.62(5) mm s^{-1} at 4.2 K (Ar and Xe matrix) and 0.63(2) mm s^{-1} at 5 K (Ar matrix),[65,67] indicating the influences of crystalline $FeCl_2$ lattice packing. Calculations herein assumed the $^5\Delta_g$ ground-state of $FeCl_2$, which has gas-phase equilibrium bond lengths determined at 2.128(7) Å.[68] Previous studies have indicated a linear equilibrium geometry and the Cl-p-orbital-π-bonding (and metal 3d polarization) interaction to make an appreciable contribution to the overall Fe−Cl bond-order, in turn indicating the requirement of adequate basis polarization.[14,69−73] Treatment of Cl with the cc-pVQZ basis gave no substantial EFG difference to cc-pVTZ, indicating the latter to give a suitable bonding description. As for CuCl, geometrical optimizations with each functional gave a large range of EFG magnitudes and even sign depending on the functional, as outlined in Table 1. In accord with the work of Schwerdtfeger et al.,[12] all functionals underestimated EFGs in comparison with experiment. A rough

Table 1. Computed EFG Parameters for Gas-Phase and Scaffold $^5\Delta_g$ $FeCl_2$[a]

functional	R(FeCl)[a]	$V_{\hat{z}\hat{z}}$	ΔE_Q[b]	$\langle S^2 \rangle$
		Gas Phase		
ROHF	2.220	0.108 (0.893)	0.16−0.17 (1.35−1.44)	
UHF	2.216	0.107 (0.893)	0.16−0.17 (1.35−1.44)	6.016 (6.019)
ROBHHLYP	2.167	0.110 (1.008)	0.17−0.18 (1.53−1.63)	
UBHHLYP	2.163	0.101 (1.010)	0.15−0.16 (1.53−1.63)	6.013 (6.012)
ROB3LYP	2.148	0.106	0.16−0.17	
UB3LYP	2.147	0.101 (1.000)	0.15−0.16 (1.52−1.62)	6.012 (6.014)
CAM-ROB3LYP	2.138	0.001 (0.959)	0.00−0.00 (1.45−1.55)	
CAM-UB3LYP	2.136	−0.005 (0.961)	0.01−0.01 (1.46−1.55)	6.010 (6.011)
CAM-ROB3LYP*	2.167	0.066 (0.980)	0.10−0.11 (1.49−1.59)	
CAM-UB3LYP*	2.163	0.057 (0.981)	0.01−0.01 (1.49−1.59)	6.012 (6.011)
ROωB97XD	2.104	−0.124 (0.961)	0.19−0.20 (1.46−1.55)	
UωB97XD	2.102	−0.134 (0.961)	0.20−0.22 (1.46−1.55)	6.010 (6.009)
ROPBE0	2.137	0.045 (0.974)	0.07−0.07 (1.48−1.58)	
UPBE0	2.136	0.043 (0.981)	0.07−0.07 (1.49−1.59)	6.013 (6.017)
ROTPSSh	2.132	0.048	0.07−0.08	
ROMP2(full)	2.139	0.052 (1.014)	0.08−0.08 (1.54−1.64)	
UMP2(full)	2.139	0.031 (1.011)	0.05−0.05 (1.53−1.63)	6.017 (6.019)
ROB2PLYP	1.985	−0.420 (1.005)	0.64−0.68 (1.52−1.63)	
		Planar Scaffold		
BHHLYP	X-ray	(0.665)	(1.01−1.08)	

[a] Calculations performed at optimized and X-ray geometries in parentheses, $V_{\hat{z}\hat{z}}$ is reported in au and ΔE_Q in units of mm s^{-1}. [b] Range of quadrupole splitting, ΔE_Q, corresponds to Q = 150−160 mb.

correlation exists between optimized bond length and EFG, showing that as different functionals optimized to a slightly longer bond length, a more positive EFG was obtained. In contrast to CuCl, B2PLYP appeared to perform worst geometrically at 1.985 Å and gave a *negative* EFG with ΔE_Q (incorrectly) at 0.64 mm s^{-1}. The incorporation of DKH2 and DKH4 relativistic corrections to BHHLYP gave a 2.8% and 1.4% decrease compared to nonrelativistic $V_{\hat{z}\hat{z}}$, respectively, as well as a optimizing to a slightly shorter bond length of 2.158 Å. It can therefore be said that the effects of relativity on the EFG appear to be small; this conclusion is also confirmed later for FCL.

These optimized bond lengths are distorted considerably compared to crystallography, which has been reported very precisely at R(Fe−Cl) = 2.530 86 Å.[62] EFG calculations were therefore performed at the X-ray geometry for two different cases: one $FeCl_2$ unit; and a central Fe atom with six surrounding iron atoms, which completes all crystallographic coordinations (denoted as the planar scaffold), giving a total of 24 chlorine atoms, an overall charge of −10, and D_{3d} symmetry with 1021 variational basis functions. Results of these calculations are also summarized in Table 1. DKH2 and DKH4 relativistic corrections to BHHLYP for the first case were again small at ∼1% and 0.9%, respectively.

These data indicate that calculations at the X-ray geometry give a near 10-fold increase in the EFG as compared to the gas-phase calculations, although the accuracy, at a geometry that is far from optimized, is difficult to assess. The question of whether the matrix in the above-mentioned matrix isolation studies perturbs the geometry and EFG has been the subject of several theoretical studies. Hartree−Fock calculations by Hagelberg, Das, and Mishra[74] and other MP2 single-Ne calculations by Schwerdtfeger et al.[12] indicate the $FeCl_2$ EFG to be essentially unperturbed by the matrix. This conclusion is in disagreement with earlier Hartree−Fock and MP4 calculations that indicated a decrease in ΔE_Q when $FeCl_2$ is encapsulated in a Ne or Ar cluster,[75,76] although as outlined by Hagelberg et al.,[74] this earlier work lacked a good basis set description and consideration of geometrical optimization in the matrix. Due to the lack of a high-level benchmark for geometrically optimized $FeCl_2$, it remains difficult to conclude if the above-mentioned matrix isolation experiments are representative of a gas-phase geometry and, therefore, of the EFG. For the purpose of this work, the calculations herein indicated both a positive EFG for the crystalline structure, which is in accord with experiment, and a significant increase in EFG magnitude when the (scaffold) crystalline environment is considered compared to an (optimized) isolation environment. Comparison of these scaffold calculations with the 4.2 K crystalline ΔE_Q is troublesome due to the Néel transition causing an abrupt change in the EFG by about 30%.[63,64] Instead, comparison to a ΔE_Q determined by extrapolation to 0 K using literature data above the Néel temperature gives the reference value of ∼1.05(5) mm s^{-1}, which would be within error of the BHHLYP planar scaffold calculation. These calculations would therefore indicate effects of lattice packing. It is noted, however, that ideally solid-state plane wave optimizations would be required for a more accurate description of this system.

Due to basis set core convergence for both CuCl and $FeCl_2$ as well as the noted agreement to previous calculations and experiments, the cc-pwCVTZ(+p2d)/cc-pVTZ bases for Fe/Cl were considered suitable for FCL EFG calculations.

3.2. $FeCl_2 \cdot 4H_2O$. Experiments have shown that ΔE_Q for FCL is essentially temperature independent: 3.10 mm s^{-1} at 4.2 K, 3.14 mm s^{-1} at 77 K, 3.02 mm s^{-1} at 300 K, and 2.994 mm s^{-1} in the Bull et al.[4] experimental EFG determination at 295 K.[34,77,78]

Ingalls et al.[34,78] determined the low temperature limiting value at 3.15 mm s^{-1}. The assumption is made here that, following the pioneering intensity tensor work of Zimmermann,[7,8] η is also temperature independent under these circumstances and provides rationale for the comparison of the experimental EFG at 295 K with 0 K calculations. The results of EFG calculations for a $FeCl_2 \cdot 4H_2O$ octahedron at the X-ray geometry, a geometrically optimized octahedron, and X-ray geometry scaffold calculations are given in Tables 2, 3 and 4, respectively.

The reference X-ray geometry has R(Fe−O1) = 2.077(1) Å, R(Fe−O2) = 2.144(2) Å, R(Fe−Cl) = 2.5266(3) Å, and all octahedron angles 92.11−87.89°.[38] All tabulated calculations given in Table 2 obtained a positive sign of $V_{\hat{z}\hat{z}}$, η between

Table 2. Computed EFG Parameters for X-ray $FeCl_2 \cdot 4H_2O$[a]

functional	$V_{\hat{z}\hat{z}}$	η	ΔE_Q[b]	$\langle S^2 \rangle$
ROHF	2.265	0.22	3.46−3.69	
UHF	2.243	0.22	3.43−3.66	6.007
ROBHHLYP	2.264	0.21	3.46−3.69	
UBHHLYP	2.248	0.22	3.44−3.66	6.006
ROB3LYP	2.183	0.22	3.34−3.56	
UB3LYP	2.169	0.23	3.32−3.54	6.005
CAM-ROB3LYP	2.210	0.22	3.38−3.60	
CAM-UB3LYP	2.197	0.22	3.36−3.58	6.005
CAM-ROB3LYP*	2.267	0.21	3.46−3.69	
CAM-UB3LYP*	2.252	0.21	3.44−3.67	6.005
ROωB97XD	2.203	0.22	3.37−3.59	
UωB97XD	2.190	0.22	3.35−3.59	6.005
ROPBE0	2.164	0.22	3.31−3.53	
UPBE0	2.148	0.23	3.29−3.50	6.005
ROTPSSh	2.151	0.19	3.28−3.50	
ROMP2(full)	2.291	0.23	3.50−3.74	
UMP2(full)	2.283	0.23	3.49−3.72	6.007
ROB2PLYP	2.266	0.21	3.46−3.69	
UB2PLYP	2.250	0.22	3.44−3.67	6.006

[a] Calculations performed at X-ray geometries, $V_{\hat{z}\hat{z}}$ is reported in au and ΔE_Q in units of mm s^{-1}. [b] Range of quadrupole splitting, ΔE_Q, corresponds Q = 150−160 mb.

Table 4. Computed EFG Parameters for Scaffold $FeCl_2 \cdot 4H_2O$[a]

functional	$V_{\hat{z}\hat{z}}$	η	ΔE_Q[b]	$\langle S^2 \rangle$
ROHF	1.983	0.25	3.07−3.27	
UHF	1.983	0.25	3.04−3.24	6.007
ROBHHLYP	2.047	0.23	3.13−3.34	
UBHHLYP	2.035	0.23	3.11−3.32	6.006
ROB3LYP	2.027	0.21	3.10−3.30	
UB3LYP	2.014	0.21	3.08−3.28	6.005
CAM-ROB3LYP	2.037	0.22	3.11−3.32	
CAM-UB3LYP	2.026	0.22	3.10−3.30	6.005
CAM-ROB3LYP*	2.046	0.23	3.13−3.34	
CAM-UB3LYP*	2.034	0.23	3.11−3.32	6.005
ROωB97XD	2.035	0.22	3.11−3.32	
UωB97XD	2.024	0.21	3.09−3.30	6.005
ROPBE0	2.003	0.21	3.06−3.26	
UPBE0	1.988	0.21	3.04−3.24	6.005
ROTPSSh	1.961	0.22	3.00−3.20	
UTPSSh	1.940	0.20	2.96−3.16	6.004

[a] Calculations performed at X-ray geometries using the scaffold described in the text, $V_{\hat{z}\hat{z}}$ is reported in au and ΔE_Q is given in units of mm s^{-1}. [b] Range of quadrupole splitting, ΔE_Q, corresponds Q = 150−160 mb.

Table 3. Computed EFG Parameters for Gas-Phase Optimized $FeCl_2 \cdot 4H_2O$[a]

functional	R(Fe−Cl)	R(Fe−O1)	R(Fe−O2)	$V_{\hat{z}\hat{z}}$	η	ΔE_Q[b]	$\langle S^2 \rangle$
ROHF	2.403	2.281	2.322	1.206	0.04	1.83−1.95	
UHF	2.400	2.281	2.320	1.240	0.04	1.88−2.01	6.008
ROBHHLYP	2.352	2.227	2.248	1.480	0.00	2.24−2.39	
UBHHLYP	2.349	2.228	2.248	1.460	0.01	2.21−2.36	6.007
ROB3LYP	2.315	2.271	2.306	1.301	0.03	1.97−2.10	
UB3LYP	2.329	2.265	2.275	1.301	0.03	1.97−2.10	6.007
ROPBE0	2.317	2.240	2.248	1.311	0.04	1.99−2.12	
UPBE0	2.314	2.241	2.249	1.292	0.04	1.96−2.09	6.007
CAM-ROB3LYP	2.353	2.233	2.253	1.382	0.04	2.10−2.24	
CAM-UB3LYP	2.325	2.225	2.233	1.363	0.04	2.07−2.20	6.006
CAM-ROB3LYP*	2.350	2.234	2.252	1.464	0.00	2.22−2.37	
CAM-UB3LYP*	2.350	2.234	2.252	1.464	0.00	2.22−2.37	6.006
ROωB97XD	2.278	2.263	2.277	1.128	0.03	1.71−1.82	
UωB97XD	2.275	2.264	2.278	1.109	0.03	1.68−1.79	6.006
ROPBE0	2.317	2.240	2.248	1.311	0.04	1.99−2.12	
UPBE0	2.314	2.241	2.249	1.292	0.04	1.96−2.09	6.007
ROTPSSh	2.310	2.248	2.249	1.297	0.07	1.94−2.06	
ROMP2(full)	2.322	2.214	2.236	1.411	0.00	2.14−2.27	
UMP2(full)	2.316	2.212	2.231	1.397	0.01	2.12−2.26	6.008
ROB2PLYP	2.205	2.230	2.239	0.848	0.09	1.29−1.37	

[a] All calculations assume a geometrical optimized geometry using the given functional, $V_{\hat{z}\hat{z}}$ is reported in au and ΔE_Q in units of mm s^{-1}. [b] Range of quadrupole splitting, ΔE_Q, corresponds Q = 150−160 mb.

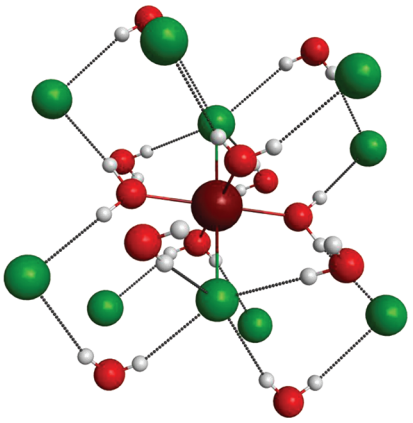

Figure 1. $FeCl_2 \cdot 4H_2O$ (FCL) scaffold showing hydrogen bonding interactions. Atoms: Fe (brown); Cl (green); O (red); H (white).

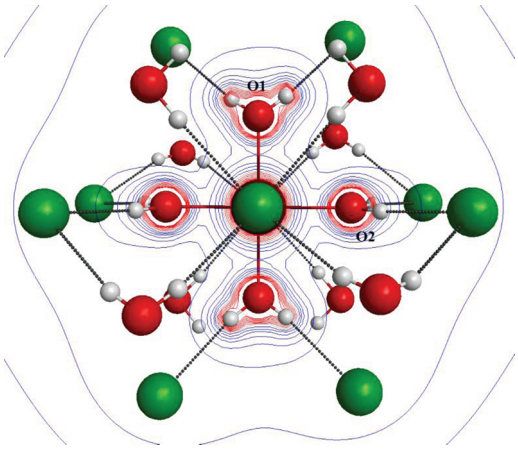

Figure 2. Two-dimensional total electrostatic potential contour projection down bond Fe−Cl.

0.19−0.23 in agreement with experiment at 0.25(2), and calculated ΔE_Q, on average, ∼7% larger than the low temperature limiting value. The positive sign of $V_{\hat{z}\hat{z}}$ is in agreement with early and experimentally difficult low-temperature magnetically perturbed studies.[79,80] The incorporation of DKH2 or DKH4 relativistic integral corrections to BHHLYP decreased the magnitude of $V_{\hat{z}\hat{z}}$ by ∼0.8%, and UHF was decreased by ∼1%. The difference between DKH2 and DKH4 treatments was less than 2 milli au in $V_{\hat{z}\hat{z}}$ in both instances.

When the X-ray geometry is allowed to geometrically optimize for each respective functional, there was on average, a 6.53 eV improvement of the total energy as well as a ∼42% decrease of ΔE_Q, with the lowest energy structure of a $FeCl_2 \cdot 4H_2O$ octahedron assuming D_{2h} point symmetry. The difference between the two optimized Fe−O bonds is small, resulting in $\eta \sim 0$. In accord with the expression for ΔE_Q, when $\eta = 0$, $(1 + \eta^2/3)^{1/2} = 1$, when $\eta = 0.20-0.25$, $(1 + \eta^2/3)^{1/2} = 1.0066-1.0104$, and when $\eta = 1$, $(1 + \eta^2/3)^{1/2} = 1.1547$. That is, when $\eta \sim 0.20-0.25$, its influence on the measurable ΔE_Q is expected to be <1%. Due to the fact that the crystalline geometry has distortion from the optimized structure, namely the R(Fe−Cl) stretch in the latter, it would be expected that optimized geometries that recover packing interactions would be more suitable.

The scaffold structure used in this work attempts to recover the major extent of interoctahedron interactions and was adapted from earlier work.[38] Briefly, the scaffold frame contains the nearest eight chloride anions and eight waters that complete all hydrogen-bonding interactions to a central complex and results in a total of 713 variational basis functions. A schematic showing the scaffold, i.e., a central $FeCl_2 \cdot 4H_2O$ octahedron in the scaffold frame, is given in Figure 1.

These scaffold calculations gave an average ΔE_Q of 3.08 mm s^{-1}, which is in excellent agreement with the Ingalls et al.[34,78] low-temperature limiting value of 3.15 mm s^{-1}, and the calculated values of η again in excellent accord with experiment. All-electron B2PLYP has a N^5 computational scaling limiting step and was too expensive to be applied for the scaffold system. The decrease in EFG magnitude for the scaffold compared with an isolated octahedron is in accord with the generally established EFG trend that valence and lattice contributions usually have opposite signs; inclusion of the scaffold interactions causes a decrease relative to the gas-phase X-ray geometry octahedron. A further apparent trend in the transition from CuCl and $FeCl_2$ to the single octahedron and finally scaffold calculations is, in accord with decreasing multireference character, the converging closeness of calculated EFGs with different functionals. Unlike CuCl or $FeCl_2$ where the electrons from one or two bonding atoms influence the metal-centered EFG and any small bonding deviation or density functional parametrization can substantially influence the EFG, the Fe nucleus in FCL experiences an averaged (ligand-saturated) electric field and hence EFG from all coordinated species, and in accord, can buffer small changes in geometry and functional parametrizations. Finally, considering energetics, $\langle S^2 \rangle$, and parameters from Tables 2−4, the largest variation in EFG between the ROKS and UKS methods for a given functional was <1%, indicating that for these calculations, spin contamination and spin polarization effects are small.

The scaffold calculations have an eigenvector angular spread of about 5° between different EFG functionals, and all reveal $V_{\hat{z}\hat{z}}$ to be almost coaxial with the shorter Fe−O1 bond, $V_{\hat{y}\hat{y}}$ with the longer Fe−O2 bond, and $V_{\hat{x}\hat{x}}$ with the Fe−Cl bond. The deviation from coaxiality occurs due to the slight solid-state distortion of the octahedron. Unfortunately, because these calculations model 0 K conditions, neglecting both zero-point and vibrational effects, a direct comparison with experimental eigenvectors is not possible. Although a small change in geometry can change the magnitudes of ΔE_Q and η, the resulting change in eigenvectors can be significantly larger. Such a change in orientation is especially true for FCL, where the crystalline ^{57}Fe nuclear expectation MSDs are both anisotropic and large (∼0.0412 × 10^{-16} cm^2 or displacement of ∼0.2 Å) at 295 K and apparently show coupled alignment with phonon modes.[4] The sensitivity of EFG orientation with FCL geometry can be visualized by considering contour plots of electrostatic density; one such plot is given in Figure 2 considering projection coaxial with the Fe−Cl bond. By eq 1 the main EFG component is directed along the path of most rapidly decreasing electric field. For FCL the field lines are relatively isotropic surrounding the iron atom, allowing a small displacement of either iron or ligand (charge contributions to the EFG radially scale as $\langle r^{-3} \rangle$) to have a substantial influence on eigenvector orientation.

To further investigate the change of EFG with changing scaffold geometry, BHHLYP stretching calculations were performed. A geometrical optimization of the central complex in a scaffold frame is difficult and not reliable for two reasons: DFT generally does not perform well for van der Waals interactions,

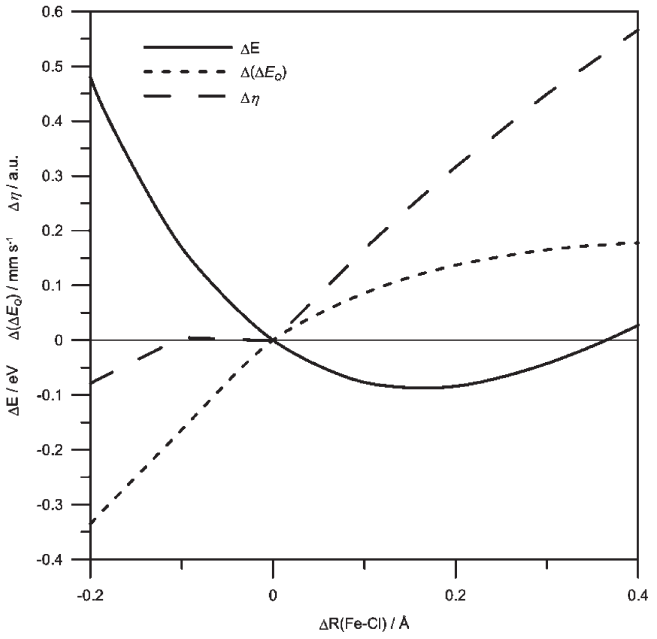

Figure 3. Change of calculated scaffold energy (E), quadrupole splitting (ΔE_Q), and asymmetry parameter (η) with R(Fe−Cl).

and the second co-ordination chloride and water species are not polarized correctly due to a lack of extended supramolecular structure. The first of these issues can in part be addressed by considering a functional that is known to perform well for hydrogen-bonding interactions, whereas fully addressing the second issue was considered to be too computationally expensive for Gaussian-basis DFT methods. The use of periodic boundary condition plane wave solid-state type calculations would be naturally suited to address this latter issue. Nevertheless, a fairer Gaussian basis comparison involved calculating BHHLYP EFG while systematically varying inner-complex bonding parameters using single-point calculations and is summarized in Figure 3.

As R(Fe−Cl) is stretched, ΔE_Q remains in experimental agreement within error, although η shows a dramatic increase toward unity, reaching the value of ∼0.50/∼0.68 (change of ∼0.30/∼0.45 in Figure 3) for a 0.2/0.3 Å stretch from the X-ray geometry. This is a consequence of the $\langle r^{-3} \rangle$ dependence of the EFG toward an oblate-like tensor determined mainly by the four coordinated water molecules. As η becomes close to unity, the sign of ΔE_Q becomes increasingly influenced by the electronic environment; i.e. $V_{\hat{x}\hat{x}}$ will be close to zero, and $V_{\hat{z}\hat{z}}$ and $V_{\hat{y}\hat{y}}$ will have similar magnitudes but opposite signs. Therefore, a small change in $V_{\hat{x}\hat{x}}$ that results in a sign change will also change the sign of $V_{\hat{z}\hat{z}}$. Calculations in this regime to correctly model EFGs would not be sensible. Compression of the Fe−Cl bond results in a decrease of ΔE_Q, an increase in energy, and a slow decrease in η, with all parameters again tending away from experimental (or lowest energy) agreement. Calculations involving orthogonalizing either first the square-planar water coordination (crystallographic angles between 88.4 and 94.8°) or the entire octahedral $FeCl_2(H_2O)_4$ structure gave a small relative energy increase of 0.27 eV, although they gave essentially no change in ΔE_Q or η. Bond stretching/compressing calculations were also performed (independently) for the two different Fe−OH_2 bonds, giving analogous observations to those for R(Fe−Cl). That is, from the scaffold point of view, the X-ray geometry is near the energy minimum, and stretching of the bond gives either a large change in η or, in the case of the Fe−O1 bond, a dramatic increase of ΔE_Q by up to ∼±0.6 for a 0.1 Å bond compression or stretch, respectively. This stretch magnitude is close to the expected isotropic MSD magnitude of the iron nucleus and oxygen atom isotropic atomic displacement parameters at 0.13 and 0.14 Å for O1 and O2, respectively.[38] Moreover, a Fe−O1 bond stretch by 0.1 Å gives R(Fe−O1) = 2.177 Å, which is now larger than R(Fe−O2) = 2.144 Å, and in consequence there is a reorientation of the EFG so that $V_{\hat{z}\hat{z}}$ is coaxial with Fe−O2. This sensitivity of eigenvectors within the expected thermal displacement at room temperature indicates the necessity of dynamical and thermal corrections for a correct description at experimental temperatures. It can be concluded from these calculations that the X-ray geometry gives near-minimized (equilibrium) scaffold energy, consistent with ΔE_Q, and yielded a value of η that is within experimental error *only near this geometry*. In turn, these calculations would appear to support the conclusion that in contrast to gas-phase EFG calculations where higher symmetry may pertain, the solid-state distortion of molecular packing and intermolecular bonding interactions plays a significant role in the measurable EFG. Hence, for a crystal lattice that has strong intermolecular interactions, it is the case that the entire unit cell contents either directly by proximity or indirectly by modifying geometry close to the ^{57}Fe nucleus influence the EFG. These conclusions could be summarized to say that a significant portion of the measurable ΔE_Q can arise, unsurprisingly, from crystalline packing at non-gas-phase geometries.

4. CONCLUSIONS

This study has demonstrated some of the challenges involved in the computation of electric-field-gradient (EFG) hyperfine parameters for transition metal species. The microscopic asymmetry parameter for ferrous chloride tetrahydrate was calculated at 0.21−0.23, which is in excellent accord with experiment at 0.25(2), with a positive sign of the EFG. These calculations also demonstrated that in systems similar to FCL, that is, where there are substantial interoctahedron interactions, accurate calculations require consideration of these interactions and their influence on the molecular geometry. By virtue of agreement of theory with experiment, this work supports the contention that consideration of simultaneous macroscopic EFG and mean-squared-displacement (MSD) data can, in favorable circumstances, yield physically meaningful microscopic EFG and MSD tensors. Finally, a natural extension of this work would be to couple periodic (plane wave) DFT calculations with molecular dynamics methods to investigate the influence of vibrational motion and temperature effects on EFG eigenvector orientation as well as species like ferrous ammonium sulfate hexahydrate that exhibit a temperature-dependent quadrupole splitting. It is hoped that this study will help motivate future work in this direction. Finally, it is hoped that more density functional development will be undertaken by theoreticians in the near future to generally improve the performance of DFT, in both relativistic and nonrelativistic approximations, for core-like properties. The explosive scaling of high-level wave function all-electron correlation treatments with the size of the system means that accurate basis set calculations on species with more than a few atoms is a formidable task.

AUTHOR INFORMATION

Corresponding Author
*E-mail: james.bull@chem.ox.ac.uk.

ACKNOWLEDGMENT

Computational resources were in part provided by the University of Canterbury BlueFern (UCSC) supercomputer facility. J.N.B. acknowledges financial support through an award of a New Zealand Tertiary Education Commission Top Achiever Scholarship during the time spent at the University of Canterbury. Prof. Peter Schwerdtfeger, Massey University, is thanked for useful discussions. We thank the unknown reviewers for useful comments and suggestions.

REFERENCES

(1) Dufek, P.; Blaha, P.; Schwarz, K. *Phys. Rev. Lett.* **1995**, *75*, 3545.
(2) Martínez-Pinedo, G.; Schwerdtfeger, P.; Caurier, E.; Langanke, K.; Nazarewicz, W.; Söhnel, T. *Phys. Rev. Lett.* **2001**, *87*, 062701.
(3) Pyykkö, P. *Mol. Phys.* **2008**, *106*, 1965.
(4) Bull, J. N.; Fitchett, C. M.; Tennant, W. C. *Hyperfine Interact.* **2010**, *198*, 273.
(5) Bull, J. N.; Robinson, W. T.; Tennant, W. C. *Hyperfine Interact.* **2009**, *194*, 347.
(6) Zory, P. *Phys. Rev.* **1965**, *140*, A1401.
(7) Zimmermann, R. *Nucl. Instrum. Methods* **1975**, *128*, 537.
(8) Zimmermann, R.; Doerfler, R. *Hyperfine Interact.* **1982**, *12*, 79.
(9) Tennant, W. C. *J. Phys.: Condens. Matter* **1992**, *4*, 6993.
(10) Schwerdtfeger, P.; Pernpointner, M.; Nazarewicz, W. Calculation of Nuclear Quadrupole Coupling Constants. In *17 Calculation of NMR and EPR Parameters: Theory and Applications*; Kaupp, M., Bühl, M., Malkin, V. G., Eds.; Wiley-VCH Verlag GmbH & Co. KGaA: Weinheim, 2004; pp 279−291.
(11) Cramer, C. J.; Truhlar, D. G. *Phys. Chem. Chem. Phys.* **2009**, *11*, 10757.
(12) Schwerdtfeger, P.; Söhnel, T.; Pernpointner, M.; Laerdahl, J. K.; Wagner, F. E. *J. Chem. Phys.* **2001**, *115*, 5913.
(13) Sinnecker, S.; Slep, L. D.; Bill, E.; Neese, F. *Inorg. Chem.* **2005**, *44*, 2245.
(14) Bast, R.; Schwerdtfeger, P. *J. Chem. Phys.* **2003**, *119*, 5988.
(15) Aquino, F.; Govind, N.; Autschbach, J. *J. Chem. Theory Comput.* **2010**, *6*, 2669.
(16) Thierfelder, C.; Schwerdtfeger, P.; Saue, T. *Phys. Rev. A* **2007**, *76*, 034502.
(17) Mastalerz, R.; Barone, G.; Lindh, R.; Reiher, M. *J. Chem. Phys.* **2007**, *127*, 074105.
(18) Kellö, V.; Sadlej, A. J. *Int. J. Quantum Chem.* **1998**, *68*, 159.
(19) Antony, J.; Hansen, B.; Hemmingson, L.; Bauer, R. *J. Phys. Chem. A* **2000**, *104*, 6047.
(20) Haliker, A.; Koch, H.; Christiansen, O.; Jørgensen, P.; Helgaker, T. *J. Chem. Phys.* **1997**, *107*, 849.
(21) Schwerdtfeger, P.; Pernpointner, M.; Laerdahl, J. K. *J. Chem. Phys.* **1999**, *111*, 3357.
(22) Nemykin, V. N.; Hadt, R. G. *Inorg. Chem.* **2006**, *45*, 8297.
(23) Bjornsson, R.; Bühl, M. *Dalton Trans.* **2010**, *39*, 5319.
(24) Bochevarov, A. D.; Friesner, R. A.; Lippard, S. J. *J. Chem. Theory Comput.* **2010**, *6*, 3735.
(25) Mastalerz, R.; Widmark, P.-O.; Roos, B. O.; Lindh, R.; Reiher, M. *J. Chem. Phys.* **2010**, *133*, 144111.
(26) Schreckenbach, G. *J. Chem. Phys.* **1999**, *110*, 11936.
(27) Kárpáti, S.; Szalay, R.; Császár, A. G.; Süvegh, K.; Nagy, S. *J. Phys. Chem. A* **2007**, *111*, 13172.
(28) Cuny, J.; Messaoudi, S.; Alonzo, V.; Furet, E.; Halet, J.-F.; Le Fur, E.; Ashbrook, S. E.; Pickard, C. J.; Gautier, R.; Le Polles, L. *J. Comput. Chem.* **2008**, *29*, 2279.
(29) Byrant, P. L.; Harwell, C. R.; Wu, K.; Fronczek, F. R.; Hall, R. W.; Butler, L. G. *J. Phys. Chem. A* **1999**, *103*, 5246.
(30) Moore, E. A.; Johnson, C.; Mortimer, M.; Wigglesworth, C. *Phys. Chem. Chem. Phys.* **2000**, *2*, 1325.
(31) Blaha, P.; Schwarz, K.; Faber, W.; Luitz, J. *Hyperfine Interact.* **2000**, *126*, 389.
(32) Petrilli, H. M.; Blöchl, P. E.; Blaha, P.; Schwarz, K. *Phys. Rev. B* **1998**, *57*, 14690.
(33) Kurian, R.; Filatov, M. *Phys. Chem. Chem. Phys.* **2010**, *12*, 2758.
(34) Ingalls, R. *Phys. Rev.* **1964**, *133*, A787.
(35) Golding, R. M. *Applied Wave Mechanics*; D. Van Nostrand Company Ltd.: New York, 1969; pp 411−423.
(36) Schmidt, M. W.; Baldridge, K. K.; Boatz, J. A.; Elbert, S. T.; Gordon, M. S.; Jensen, J. H.; Kosecki, S.; Matsunaga, N.; Nguyen, K. A.; Su, S.; Windus, T. L.; Dupuis, M.; Montgomery, J. A., Jr. *J. Comput. Chem.* **1993**, *14*, 1347.
(37) CFOUR, Coupled-Cluster techniques for Computational Chemistry, a quantum-chemical program package by Stanton, J. F.; Gauss, J.; Harding, M. E.; Szalay, P. G. with contributions from Auer, A. A.; Bartlett, R. J.; Benedikt, U.; Berger, C.; Bernholdt, D. E.; Bomble, Y. J.; Christiansen, O.; Heckert, M.; Heun, O.; Huber, C.; Jagau, T.-C.; Jonsson, D.; Jusélius, J.; Klein, K.; Lauderdale, W. J.; Matthews, D. A.; Metzroth, T.; O'Neill, D. P.; Price, D. R.; Prochnow, E.; Ruud, K.; Schiffmann, F.; Stopkowicz, S.; Vázquez, J.; Wang, F.; Watts, J. D. and the integral packages MOLECULE (Almlöf, J.; Taylor, P. R.), *PROPS* (Taylor, P. R.), *ABACUS* (Helgaker, T.; Jensen, H. J. Aa.; Jørgensen, P.; Olsen, J.), and ECP routines by Mitin, A. V.; van Wüllen, C. For the current version, see http://www.cfour.de.
(38) Bull, J. N.; Maclagan, R. G. A. R.; Fitchett, C. M.; Tennant, W. C. *J. Phys. Chem. Solids* **2010**, *71*, 1746.
(39) Dunning, T. H., Jr. *J. Chem. Phys.* **1989**, *90*, 1007.
(40) Wilson, A. K.; van Mourik, T.; Dunning, T. H., Jr. *J. Mol. Struct. (THEOCHEM)* **1998**, *388*, 339.
(41) Woon, D. E.; Dunning, T. H., Jr. *J. Chem. Phys.* **1993**, *98*, 1358.
(42) Balabanov, N. B.; Peterson, K. A. *J. Chem. Phys.* **2005**, *123*, 064107.
(43) Schäfer, A.; Huber, C.; Ahlrichs, R. *J. Chem. Phys.* **1994**, *100*, 5829.
(44) Frisch, M. J.; Trucks, G. W.; Schlegel, H. B.; Scuseria, G. E.; Robb, M. A.; Cheeseman, J. R.; Scalmani, G.; Barone, V.; Mennucci, B.; Petersson, G. A.; Nakatsuji, H.; Caricato, M.; Li, X.; Hratchian, H. P.; Izmaylov, A. F.; Bloino, J.; Zheng, G.; Sonnenberg, J. L.; Hada, M.; Ehara, M.; Toyota, K.; Fukuda, R.; Hasegawa, J.; Ishida, M.; Nakajima, T.; Honda, Y.; Kitao, O.; Nakai, H.; Vreven, T.; Montgomery, J. A., Jr.; Peralta, J. E.; Ogliaro, F.; Bearpark, M.; Heyd, J. J.; Brothers, E.; Kudin, K. N.; Staroverov, V. N.; Kobayashi, R.; Normand, J.; Raghavachari, K.; Rendell, A.; Burant, J. C.; Iyengar, S. S.; Tomasi, J.; Cossi, M.; Rega, N.; Millam, N. J.; Klene, M.; Knox, J. E.; Cross, J. B.; Bakken, V.; Adamo, C.; Jaramillo, J.; Gomperts, R.; Stratmann, R. E.; Yazyev, O.; Austin, A. J.; Cammi, R.; Pomelli, C.; Ochterski, J. W.; Martin, R. L.; Morokuma, K.; Zakrzewski, V. G.; Voth, G. A.; Salvador, P.; Dannenberg, J. J.; Dapprich, S.; Daniels, A. D.; Farkas, Ö.; Foresman, J. B.; Ortiz, J. V.; Cioslowski, J.; Fox, D. J. *Gaussian 09*, Revision A.1; Gaussian, Inc.: Wallingford, CT, 2009.
(45) Douglas, M.; Kroll, N. M. *Ann. Phys.* **1974**, *82*, 89.
(46) Hess, B. A. *Phys. Rev. A* **1985**, *32*, 756.
(47) Hess, B. A. *Phys. Rev. A* **1986**, *33*, 3742.
(48) Jansen, G.; Hess, B. A. *Phys. Rev. A* **1989**, *39*, 6016.
(49) Barysz, M.; Sadlej, A. J. *Theor. Chem. Acc.* **1997**, *97*, 260.
(50) Becke, A. D. *J. Chem. Phys.* **1993**, *98*, 1372.
(51) Becke, A. D. *J. Chem. Phys.* **1993**, *98*, 5648.
(52) Yanai, T.; Tew, D. P.; Handy, N. C. *Chem. Phys. Lett.* **2004**, *393*, 51.
(53) Adamo, C.; Barone, V. *J. Chem. Phys.* **1999**, *110*, 6158.
(54) Chai, J.-D.; Head-Gordon, M. *Phys. Chem. Chem. Phys.* **2008**, *10*, 6615.
(55) Tao, J.; Perdew, J. P.; Staroverov, V. N.; Scuseria, G. E. *Phys. Rev. Lett.* **2003**, *91*, 146401.

(56) Grimme, S. *J. Chem. Phys.* **2006**, *124*, 034108.
(57) Zhao, Y.; Truhlar, D. G. *J. Chem. Theory Comput.* **2005**, *1*, 415.
(58) Calaminici, P. *Chem. Phys. Lett.* **2003**, *374*, 650.
(59) Kossmann, S.; Kirchner, B.; Neese, F. *Mol. Phys.* **2007**, *105*, 2049.
(60) Römelt, M.; Ye, S.; Neese, F. *Inorg. Chem.* **2009**, *48*, 784.
(61) Hoeft, J.; Lovas, F. J.; Tiemann, E.; Törring, T. *Z. Naturforsch.* **1971**, *26A*, 240.
(62) Pasternak, A. *J. Phys. C: Solid State Phys.* **1976**, *9*, 2987.
(63) Ono, K.; Ito, A.; Fujita, T. *J. Phys. Soc. Jpn.* **1964**, *19*, 2119.
(64) Hazony, Y.; Ok, H. N. *Phys. Rev.* **1969**, *188*, 591.
(65) Litterst, F. J.; Schichl, A.; Kalvius, G. M. *Chem. Phys.* **1978**, *28*, 89.
(66) Klumpp, W.; Hoffmann, K. W. *Z. Phys.* **1969**, *227*, 254.
(67) McNab, T. K.; Carstens, D. H. W.; Gruen, D. M.; McBeth, R. L. *Chem. Phys. Lett.* **1972**, *13*, 600.
(68) Hargittai, M.; Subbotina, N. Y.; Kolonits, M.; Gershikov, A. G. *J. Chem. Phys.* **1991**, *94*, 7278.
(69) Mishra, K. C.; Duff, K. J.; Kelires, P.; Mishra, S. K.; Das, T. P. *Phys. Rev. B* **1985**, *32*, 58.
(70) Wang, S. G.; Schwarz, W. H. E. *J. Chem. Phys.* **1998**, *109*, 7252.
(71) Hazony, Y.; Axtmann, R. C.; Hurley, J. W., Jr. *Chem. Phys. Lett.* **1968**, *2*, 440.
(72) Bridgeman, A. J. *J. Chem. Soc., Dalton Trans.* **1997**, 4765.
(73) Hodges, P. J.; Ashworth, S. H.; Beattie, I. R.; Brown, J. M. *Chem. Phys. Lett.* **2006**, *422*, 160.
(74) Hagelberg, F.; Das, T. P.; Mishra, K. C. *Phys. Rev. B* **2001**, *65*, 014425.
(75) Bominaar, E. L.; Guillin, J.; Marathe, V. R.; Sawaryn, A.; Trautwein, A. X. *Hyperfine Interact.* **1988**, *40*, 111.
(76) Bominaar, E. L.; Guillin, J.; Sawaryn, A.; Trautwein, A. X. *Phys. Rev. B* **1989**, *39*, 72.
(77) Brunot, B. *J. Chem. Phys.* **1974**, *61*, 2360.
(78) Lang, L. G.; De Benedetti, S.; Ingalls, R. I. *J. Phys. Soc. Jpn.* **1962**, *17B*, 131.
(79) Ono, K.; Shinohara, M.; Ito, A.; Fujita, T.; Ishigaki, A. *J. Appl. Phys.* **1968**, *39*, 1126.
(80) Grant, R. W.; Wiedersich, H.; Muir, A. H., Jr.; Gonser, U.; Delgass, W. N. *J. Chem. Phys.* **1966**, *45*, 1015.